System for space materials evaluation in LEO environment

P. Gordo [a], T. Frederico [a], R. Melicio [b,c,*], S. Duzellier [d], A. Amorim [a]

[a] CENTRA, Faculdade de Ciências da Universidade de Lisboa, Lisboa, Portugal
[b] ICT, Departamento de Física, Escola de Ciências e Tecnologia, Universidade de Évora, Portugal
[c] IDMEC, Instituto Superior Técnico, Universidade de Lisboa, Portugal
[d] ONERA the French Aerospace Lab, France

Abstract

This paper describes the conception and experimental setup of a new concept for a Vacuum Ultraviolet with extreme Thermal Vacuum Cycle system and the evaluation of LEO satellites materials with the equipment. The system was developed in the framework of a study of spacecraft debris generation due to satellites materials degradation, when exposed to space environment. The study was developed in the framework of an ESA project. Its main purpose was to evaluate the characteristics and the quantity of debris resulting from surface of satellites due spacecraft materials degradation and provide input to space debris models. The experimental setup developed partially simulates the space environment, on an accelerated mode, as endured by a spaceship in Low Earth Orbit, allows the testing of materials to a Vacuum, Ultraviolet and thermal cycles. This thermal cycling provided to the sample holder was implemented using an innovative mechanical thermal switching architecture. This architecture allows temperature cycling of +200 °C to −200 °C without the use of LN$_2$. The experimental setup design, manufacture and final characterization is presented.

© 2020 COSPAR. Published by Elsevier Ltd. This is an open access article under the CC BY-NC-ND license (http://creativecommons.org/licenses/by-nc-nd/4.0/).

Keywords: LEO; Space simulation; Thermal vacuum cycle; TVC; Vacuum ultraviolet; VUC; Space debris

1. Introduction

Space environment extends beyond the Earth´s atmosphere, already being considered as an extension of current business and domestic environmental (Williamson, 2004). The space environment is a harsh environment and the materials exposed like the spacecraft's external surfaces (e.g. MLI, paints) are subject to degradation (Anwar et al., 2018; Silverman, 1995; Samwel et al., 2019). In the case of the LEO satellites, the materials degradation can be caused by the following threats: charged particle radia-

tion, ultraviolet radiation; atomic oxygen (Banks et al., 2004); temperature extremes and cycling; micrometeoroid or debris impacts (Anwar et al., 2018). Therefore, selecting a material for a specific application becomes a difficult task (Fayazbakhsh and Abedian, 2010). The relative impact of the individual threats depends on the type of mission, its duration, the solar cycles, solar events and the orbit in which the spacecraft will be placed. To partial simulate this environment a VUVTC system that is able to expose materials to temperature cycling and to VUV radiation in vacuum, was developed. The development of the VUVTC is reported in this paper.

The main motivation to conception and experimental setup develop this facility was to carry out a study evaluate the amount of debris generated due to the space materials degradation, when exposed to space environment for periods that goes beyond the time of life of the spacecraft.

* Corresponding author at: ICT, Departamento de Física, Escola de Ciências e Tecnologia, Universidade de Évora, Portugal.
E-mail addresses: prgordo@fc.ul.pt (P. Gordo), tdfrederico@fc.ul.pt (T. Frederico), ruimelicio@gmail.com (R. Melicio), sophie.duzellier@onera.fr (S. Duzellier), aamorim@sim.ul.pt (A. Amorim).

Nomenclature

ATOX	Atomic oxygen
CFRP	Carbon fiber reinforced polymer
EOS	Earth-Observing Satellites
ESA	European Space Agency
ESD	Electrostatic discharge
ESH	Equivalent space solar exposure hours
ESTEC	European Space Research and Technology Centre
ESV	Equivalent sun hour
FCUL	Faculdade de Ciências da Universidade de Lisboa, Portugal
ITO	Indium tin oxide
HTD	High temperature dwelling
LEO	Low Earth Orbit
MAP	European space paints supplier
MLI	Multilayer insulation
MSFC	Marshall Space Flight Center
NASA	National Aeronautics and Space Administration
ONERA	French Aeronautics, Space and Defense Research Lab
PSA	Pressure sensitive adhesive tape
PSB/PUK	Thermal control coatings for satellites
TVC	Thermal vacuum cycling
VUV	Vacuum Ultra-Violet
VUVTC	Vacuum Ultraviolet with Thermal Vacuum Cycle Capabilities

---

The results (e.g. debris size distribution) serve as an input for improvement of the "MASTER 2009" model (Flegel et al., 2011). It is assumed that LEO refers to orbits in the 160 km to 1000 km altitude range, which includes the main EOS. A vehicle in LEO will receive radiant thermal energy from three primary sources: the incoming solar radiation (associated with the solar constant); Reflected solar energy resulting from the Earth albedo; Outgoing longwave radiation emitted by the Earth and atmosphere. The satellite surface temperatures can range from $-150\ °$C to 150 °C, dependent on the surface material thermo-optical properties and sun light or no sun light exposure. A spacecraft in LEO typically moves in and out of the Earth eclipse once every orbit in excess of roughly one hour.

In the case of ultraviolet solar radiation, the wavelength range with highest intensity in LEO ranges between 100 nm and 400 nm, which corresponds to a small portion of the solar spectral irradiance curve, as measured above Earth's atmosphere (Silverman, 1995). Of the entire UV spectrum, the VUV radiation (100 nm–200 nm) induces most of the satellite external surfaces degradation. In the space industry, for LEO satellites, it is common to test the materials against atomic oxygen followed by exposure to VUV and submission to thermal cycles (Gouzman et al., 2010). The 300 km environment actual composition is given in Table 1.

The spacecraft usually is partially covered with MLI. The purpose of MLI is to thermal isolate the satellite. Acting as radiation barrier and decreasing heat losses. MLI is a stack of thin polymeric layer (5–25 foils), separated by spacer or mesh or embossed crinkled. Although there are several options for the selection of the external MLI polymeric material it quite common to use Kapton film (any hydro carbonated polymers) on the external layer (aluminized-Kapton film). The Kapton is a polyimide film developed by DuPont in the late 1960 s that remains stable across a wide range of temperatures, from $-269\ °$C to 400 °C ($-452\ °$F to 752 °F; 4 K to 673 K) (Clair et al., 1980; Navick et al., 2004). Kapton is used in, among other things, flexible printed circuits (flexible electronics) and thermal blankets used on spacecraft, satellites, and various space instruments, and the aluminized-kapton film (Al-kapton) is a high performance, high-temperature resistant aluminized polyimide film, formed by sputtering aluminum onto polyimide using an aluminum vacuum deposition method. The kapton exposed to ATOX shows surface presenting cone-shape rugosity, becoming opaque; Absorptance strongly increases while Emittance decreases due to mass loss (eroded thickness) (Tighe et al., 2009). In the past there have been cases of satellites failures due to the satellite external material degradations and respective change in thermos-optical properties. Midori–II, EO satellite, has stopped working in 2003 possible due to X-ETFE degradation (change in the thermo-optical properties) due to UV (Mori and Ishizawa, 2013).

AO erosion mechanism is complex. In kapton film, erosion results from: 1) formation of CO and CO_2 volatile products (independent of temperature); 2) H abstraction (temperature dependent); 3) VUV degradation only intervenes in generating chain scissions. Therefore, it is surprising that the combination of all these mechanisms on a same material leads to variable results depending on ground simulation conditions.

Temperature is at play in the kinetics of desorption volatile products and at promoting VUV/dose degradation of polymers via the enhanced mobility of chains. VUV induces chain scission and therefore potentially also promote degradation via desorption process (Kiefer and Orwoll, 1987).

The ATOX exposure test facility, are limited and expensive (apparatus is complex). The most well-known facilities are: ESTEC, Noordwijk, the Netherlands; NASA Marshall Space Flight Center (MSFC); Space Environmental since AO Effects Lab in Alabama, USA; and Integrity Testing Laboratory (ITL) in Ontario, Canada.

Table 1
300 km environment actual composition.

Species	Density (cm^3)	Flux (Atoms/cm^{2}s)	Energy (eV)
O	$5 \cdot 10^8$	$4 \cdot 10^{14}$	5.3
O2	$1.2 \cdot 10^7$	10^{13}	10.6
O+	10^5	$8 \cdot 10^{10}$	5.3
O2+	10^4	$8 \cdot 10^9$	10.6
UV (175 nm–190 nm)	$3 \cdot 10^{-3}$ mW/m^2		

To simulate high exposure doses the ATOX test will require several days of testing while VUV and TVC may reach to one month of testing (for simulating larger doses). To overcame the limited availability of ATOX test facilities, a usually test approach, for space materials, is to make exposure in sequence: ATOX (in one of the facilities previously cited) exposure followed by VUV and TVC.

For the purpose of performing the long VUV and TVC testing, an experimental setup system with a Vacuum Ultraviolet and Thermal Vacuum Cycle Capabilities was developed. Its development steps and characterization are reported in this paper. The system was successfully used in test for an ESA project Space Debris from Spacecraft Degradation Products (project contract reference 4000113047/14/NL/EF/TU-IAS). Currently the developed system is available for further material testing campaign. The paper is structured as follows. Section 2 presents overall system architecture. Section 3 presents the system design. Section 4 reports the system performance. Section 5 presents the materials evaluation: LEO samples test flow; materials specifications; test specifications and results of the tests Section 6 outlines the conclusion.

2. System architecture

The main parts of the developed VUVTC system are:

- A vacuum subsystem; Vacuum chamber and pump system;
- A thermal switching subsystem (i.e., a thermal cycling subsystem), that heats and cools the sample holder;
- A VUV subsystem, which irradiates the sample holder with VUV radiation (100 nm–200 nm).
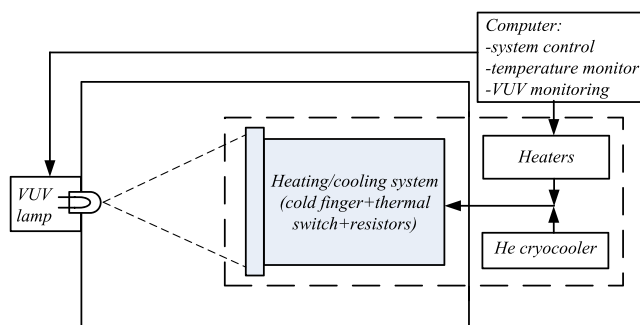

Fig. 1. TVC + VUV system architecture.

Both the thermal cycling and the VUV subsystems are in the vacuum chamber and they act on the sample holder, exposing the test materials to VUV radiation and to thermal cycles.

Special focus is given to the thermal switching subsystem due to its innovative implementation. The system architecture is shown in Fig. 1.

3. System design

3.1. Vacuum subsystem

The vacuum chamber is a stainless steel cylinder with a length of 986 mm and a radius of base of 321 mm. The vacuum pumping mechanism consists on a turbomolecular vacuum pump used to obtain and maintain a pressure inside the chamber under 10 mb–6 mb monitored by a vacuum sensor (Edwards Wide Range Gauge).

3.2. Thermal vacuum cycling subsystem

The TVC subsystem aims to provide the temperature cycling to a sample holder. In order to do so, it is necessary to have: a hot source; a cold source; thermal switching mechanism; and good thermal isolation between the sample holder and the vacuum chamber. The architecture of the TVC subsystem (Frederico, 2017) is shown in Fig. 2.

The selected architecture is based on: A He cryocooler (as cold source, 80 K), resistor as hot source and an innovative mechanical thermal switch. The mechanical thermal switches can provide physical or nonphysical contact between the cooper pistons (that are connected to the cold source) and the base plate (where the sample holder is assembled). During the heat up the mechanical thermal switches are recoiled and the resistors are turned on, heating up the AA5083 baseplate and the sample holder. During cool down the heaters are off, and the mechanical thermal switches are mechanical drives the cooper pistons, pressing them against the back of the baseplate.

The mechanical thermal switch cad design (Frederico, 2017) is shown in Fig. 3.

To reach the highest temperature the piston surfaces disengaged (i.e. moved backwards) and the heaters (thin kapton heaters) are turned on.

One of the major concerns was the contact thermal resistance between the interfaces of the pistons and the base plate. To minimize this resistance (that has an estimated
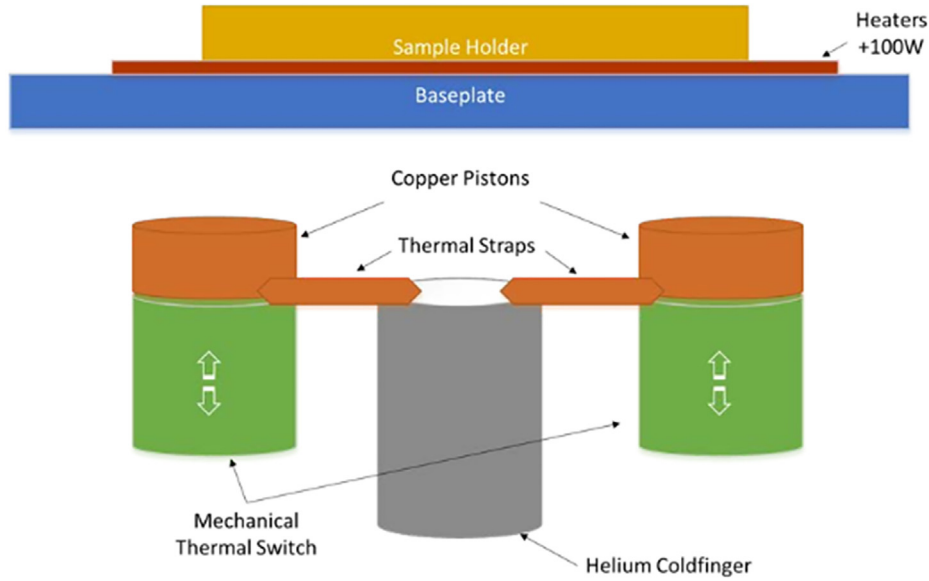
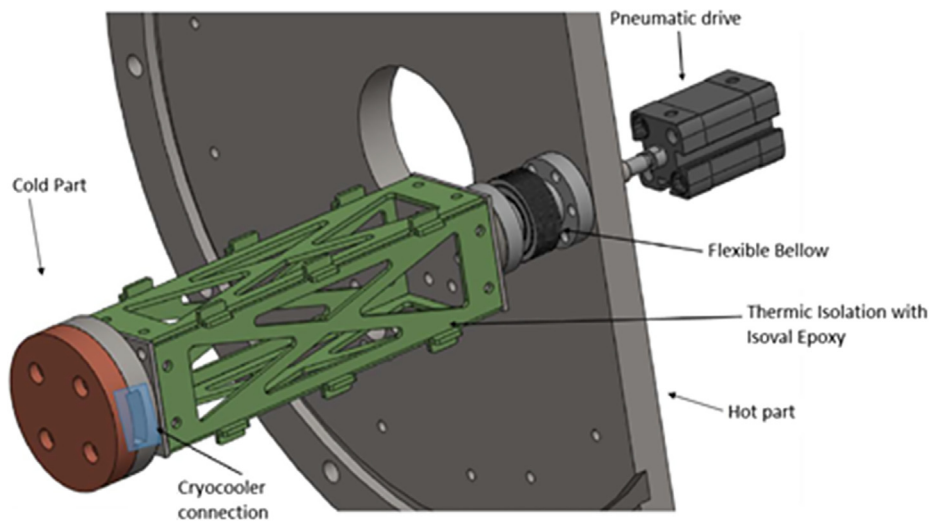Fig. 2. Architecture of the TVC subsystem (Frederico, 2017).

Fig. 3. Mechanical thermal switch design (Frederico, 2017).

value of 19 m²K/W between each piston and the base plate) the contact area in the interface was maximized and polished.

The pistons are assembled on a ball joint to allow angle adjustment and maximize the contact with the base plate. The thermal straps cross section (e.g. number of thermal straps) was maximized to ensure maximum thermal conductivity. Fig. 4 shows in more detail the 3D mechanical design of the piston.

The head of the piston is made of cooper, and its mass act as heat reservoir. When the piston is not in contact with the baseplate is still connected to the cold finger, and therefore eventually will reach the temperature of the cold finger. When the piston is driven to come in contact with
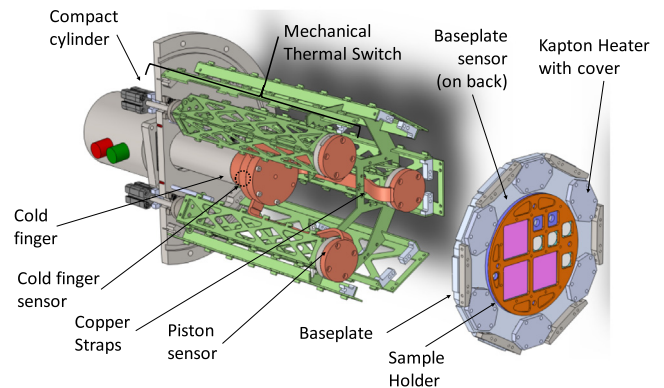
Fig. 4. 3D full mechanical implementation of the TVC subsystem (Frederico, 2017).

the baseplate it will rapidly absorb the heat from the base plate. By using this mechanism one can rapidly take heat from the baseplate and overcome power limitations of the cold finger.

The green parts in the Fig. 4 is low thermal conductive epoxy (ISOVAL epoxy), the interface with the cold piston and with the mechanical driving mechanism. This thermal isolating epoxies allows mechanical support of the piston as well thermal isolation. Heat flow of each Isoval structure is below 0.02 W for the piston (when operating at −150 °C) to the room temperature vacuum system flange. The mechanical switches consist in compressed air pneumatic (1 bar of pressure in 0.2 cm^2) drive and a flexible bellow, this works as a linear vacuum feedthrough. The force made by which pistons on the base plate is about 20 N.

Furthermore, the cold finger is able to extract 90 W of power at a temperature of −150 °C (123.15 K).

The temperature measurement and control is achieved by monitoring the sample holder temperature with PT100 sensors. These sensors were driven by Omega temperature controllers, which in turn was controlled by a computer.

The 3D full mechanical implementation of the TVC subsystem (Frederico, 2017) is shown in Fig. 4.

One cold finger and three pistons solution were implemented.

3.3. VUV subsystem

The VUV subsystem takes care of illuminating the sample holder with VUV radiation (100 nm to 200 nm). The subsystem was designed taking into account the diameter of the sample holder and the divergence of the VUV lamp. The VUV illumination subsystem architecture (Pascoal, 2016) is shown in Fig. 5.

Taking into account that the emission angle of the VUV lamp, i.e., beam angle is around $\alpha = 10°$ and the sample illuminated diameter D = 16 cm, the distance l = 90 cm.

The setup with the connection interface between the lamp and the vacuum chamber is shown in Fig. 6.

In Fig. 6 the subsystem is composed by a lamp power supply (1), the VUV lamp (Deuterium Lamp L11798 from Hamamatsu) (2), the connection interface between the lamp and the vacuum chamber (3), the vacuum chamber (4), the sample holder (5). The connection interface (Fig. 6) is essential, because during the tests it is necessary to remove the lamp for cleaning it, without breaking vacuum in the main vacuum chamber.
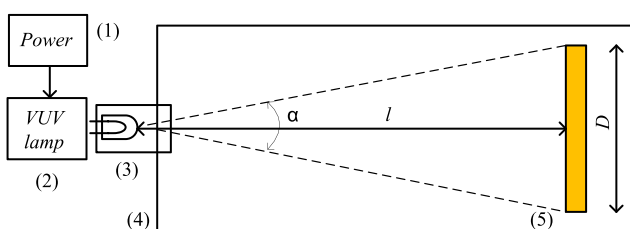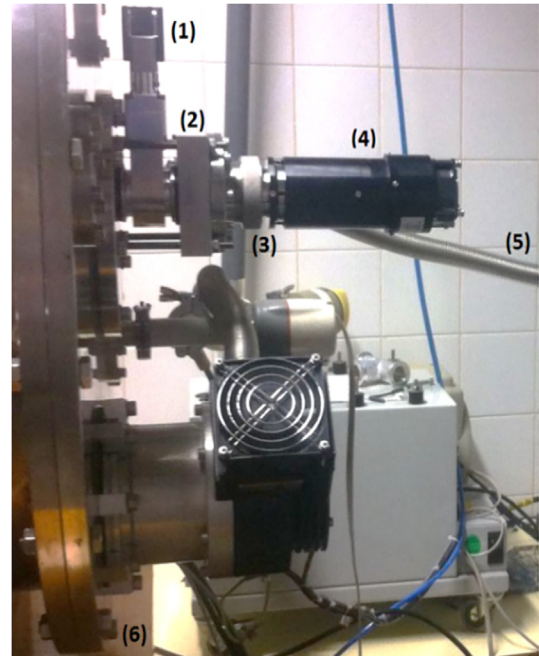

Fig. 6. Setup with the connection interface between the lamp and the vacuum chamber.

The cleaning process has to be carried out due to the deposition of a layer of material in the window of the lamp causing an irradiance decrease on the samples over the time. The contamination is expected to result from the photochemical deposition of the materials that result from the outgassing of the vacuum system. During cleaning the lamp optical irradiance at 90 cm distance is measured, for control.

4. System performance

4.1. TVC subsystem

Each TVC cycle has four phases: Warm-Up (**D** in Fig. 7), HTD (High temperature dwelling; (**A** in Fig. 7), Cool Down (**B** in Fig. 7), and Low Temperature Dwelling (**C** in Fig. 7), is shown in Fig. 7.

In the Fig. 4, it is possible to see the location of the temperature sensors in the top of the pneumatics, on the cold finger (blue) and on the sample holder (yellow).

To execute the system thermal characterization (e.g. heating rates, cooling rates), several full cycles were performed, in which the temperature of the sensors was recorded. In Fig. 7, a full cycle with a temperature range from + 150 °C to −150 °C is presented. The cycle starts in the HTD phase. In yellow is the temperature of the base plate (i.e. sample holder) and in blue, the cryocooler. The other three lines, PA, PB and PC, in green, orange and grey, respectively, are the temperatures of the pistons during the cycles. These last three sensors should measure similar temperatures, however display different values due to a variety of possible factors: different wire length, meaning

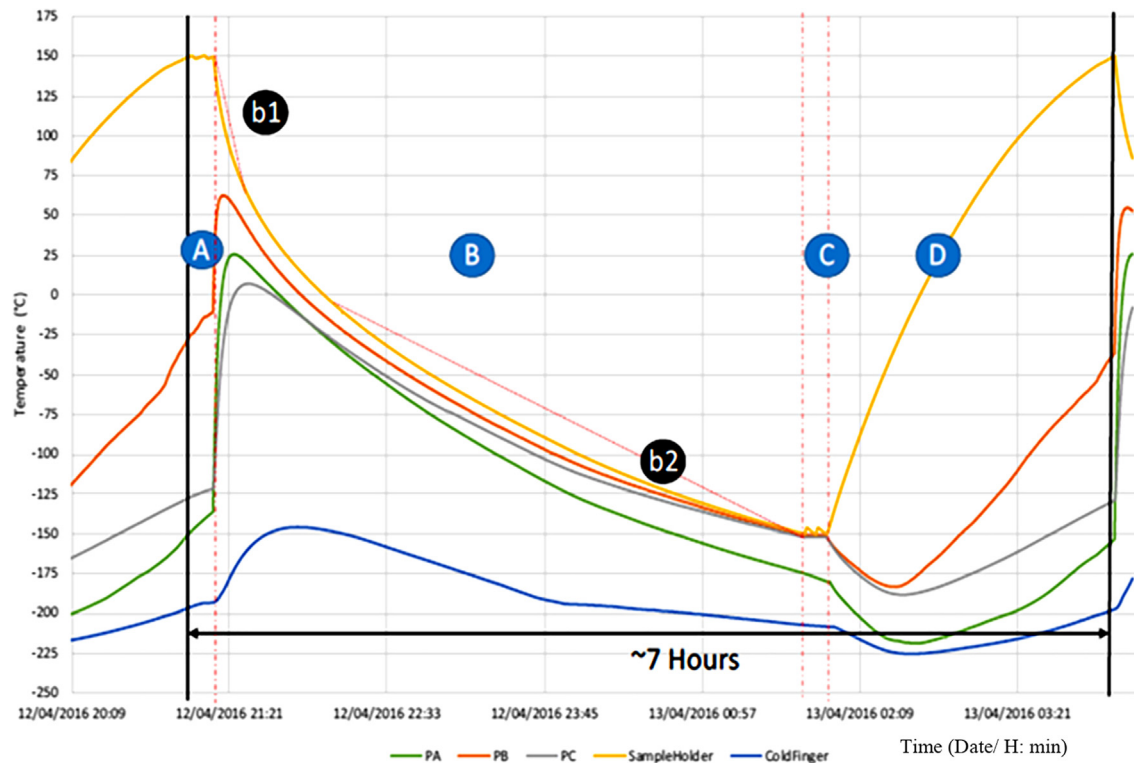Fig. 5. VUV illumination subsystem architecture (Pascoal, 2016).

Fig. 7. Temperature profiles of a thermal vacuum cycle. Each TVC cycle has four phases: HTD (A); cool down (B); low temperature dwelling (C); warm-up (D).

the compensation of the PT100 is off; bad thermal connection between the piston and the sensor.

It can be seen during Cooldown, represented by B in Fig. 7, two different cooling process taking effect, creating two different linear zones (B1 and B2 in Fig. 7). In B1, the cooling process is dominated by the thermal mass of the copper pistons, and in B2, the heat transfer is depending on the copper straps (that connects the cold finger with the cooper pistons, see Fig. 4). The cooling down rates achieved were −5.8 °C/min and −0.8 °C/min in B1 and B2 phases, respectively. The Warm-Up, D in Fig. 7, has a heat rate of +5.6 °C/min. The heating of the system is achieved only with the 100 W kapton resistors. It is possible to observe that each cycle with this temperature range takes about 7 h to complete. Other temperature ranges were tested. During this test the sample holder and the samples were not assembled, this means that the times per cycle would tend to increase during final test, the cycle duration was considered too long, and optimization was needed.

4.2. Optimization

The solution to the problem introduced was to merge the sample holder with the base plate, which resulted in the reduce of the mass. Also, the thickness of the aluminum piece that holds the kapton resistors was reduced. The total mass is now less than 764 g, when it was 2.14 kg. The 3D representation of the base plate, in which pockets were made, with different depths is shown in Fig. 8.

Due to this system change, two finite element analyses were performed, one to observe the thermal gradient (during the thermal switch activation) and the other the displacement. Both studies were retrieved from a transient study, where the whole base plate was at +150 °C and then was applied −150 °C to the areas where the pistons touch the base plate is shown in Fig. 9.

In Fig. 9(a) is shown that the thermal gradient appears to be uniform despised the reduction on the section area. In Fig. 9(b) is shown that the maximum displacement is less than 200 μm. Based on this simulation a new base plate was produced.

To execute the thermal characterization, it was repeated the process used in the first characterization with similar set of temperatures ranges and without the samples too. With the optimization of the base plate and the exchanging of the temperature range it was possible to reduce about 2 h of its initial 7 h, as shown in Fig. 10.

4.3. VUV subsystem

In the beginning of test (beginning of the lamp life) the VUV irradiance was 4.17x10-5 W/cm², at a distance of 88.96 cm.

The VUV number of suns is given by de ratio between the previous irradiance value and the irradiance of the solar spectrum AM0 (air mass zero) for the range of
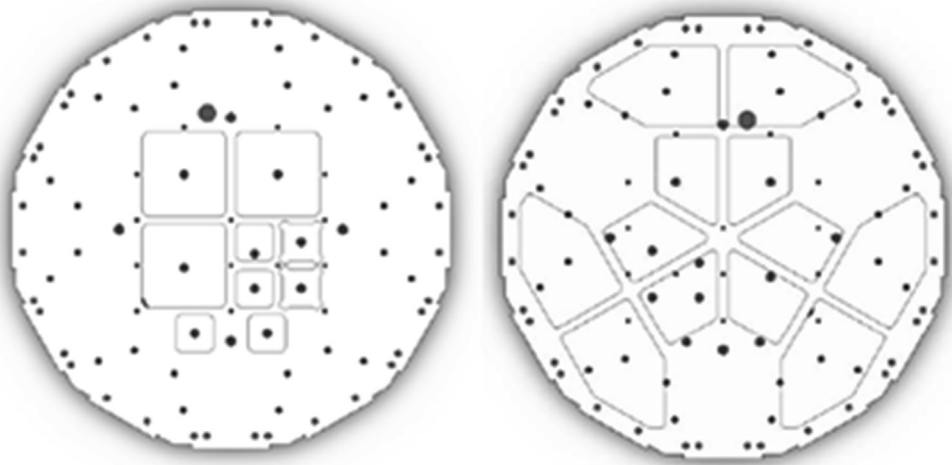
Fig. 8. On the left side is the front side of the base plate, in which the samples are placed, as well as the heat resistors. On the right, are shown the pockets on the back side.
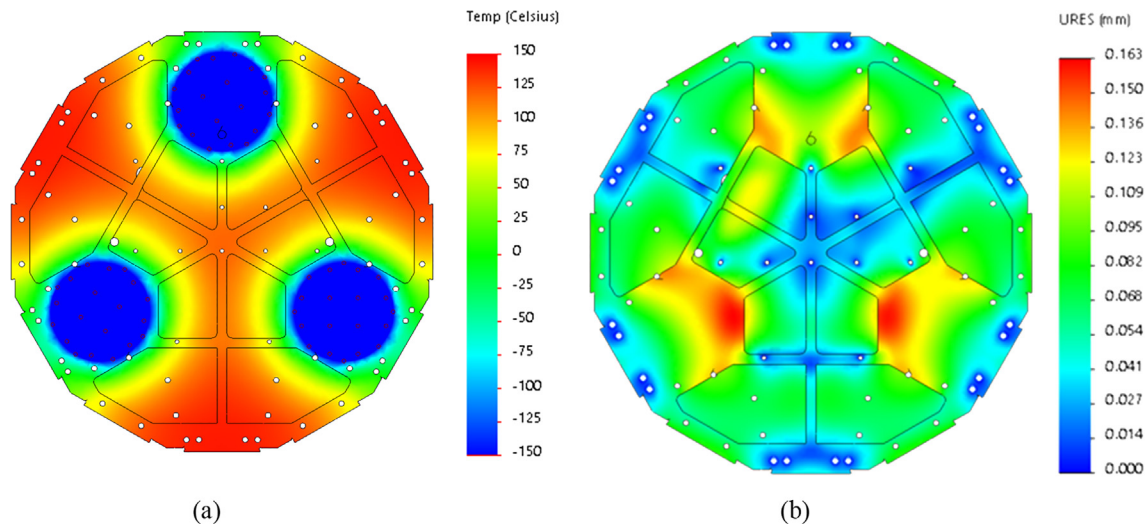

Fig. 9. (a), plot temperature gradient on the base plate. (b), deformation based on the same temperature gradient as the (9a).

wavelength between 115 nm and 200 nm. For reference, this irradiance of the solar spectrum, in the top of the atmosphere, for that range is 1.073×10^{-5} W/cm^2. For the irradiance value referred previous-ly, the equivalent value is 3.89 suns.

5. Materials evaluation

5.1. LEO samples test flow

The materials evaluation was performed in the developed system, in the frame of ESA project Space Debris from Spacecraft Degradation Products (Gordo, 2017). The aim of the project was to study the materials degradation beyond the satellite lifetime, and formation of debris due to the long-term exposure. This aim was achieved by exposing the space materials to high "doses" (i.e. high dose of ATOX, high dose of VUV and high number of TVC) of simulated environment.

The study consisted in the following major tasks:

1) Identification of the most relevant space environment conditions for LEO most populated orbits;
2) Survey and selection on most relevant representative materials, i.e. most used external spacecraft materials;
3) Test of the selected space materials, i.e., tests in simulated long term LEO environment.

The LEO space materials environmental testing was conceived to simulate the following LEO space conditions: 9.7 years; 800 km high, 75° orbit. The test flow is shown in Fig. 11.

In Fig. 11 the text box "*Initial sample characterization*" addresses the initial materials inspection, which included photos and mass determination; the text box "*ATOX*" addresses samples exposure to atomic oxygen; the "*Intermediary sample characterization*" is the intermediary inspection of the material sample for evaluation by photos
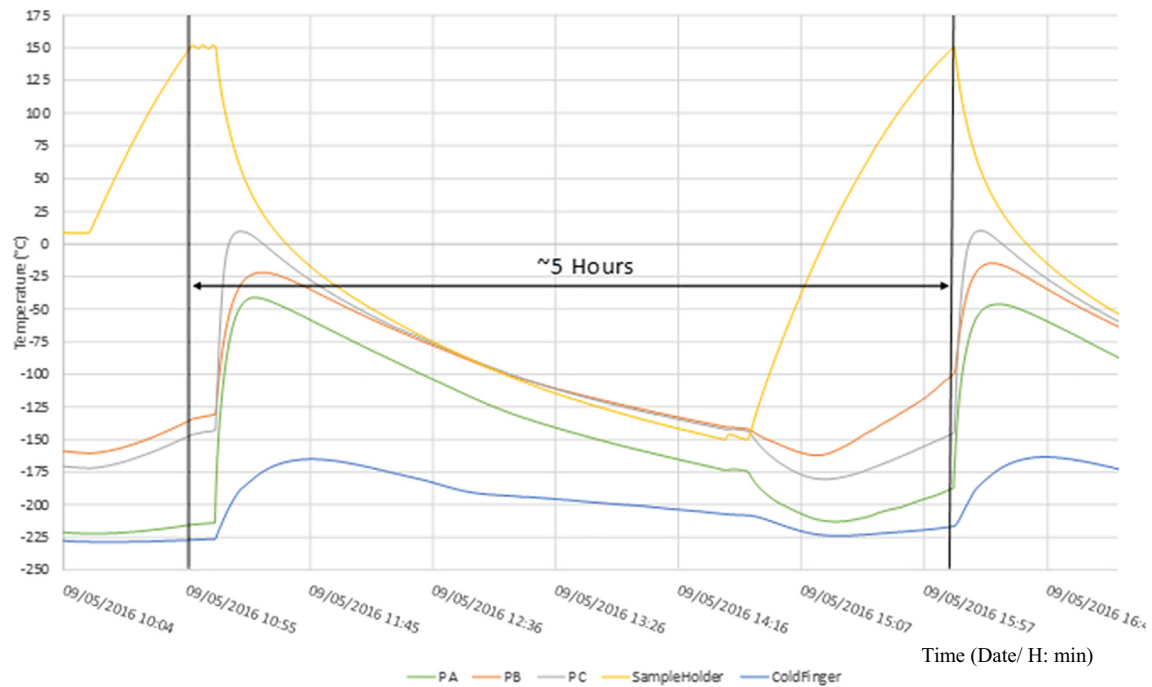
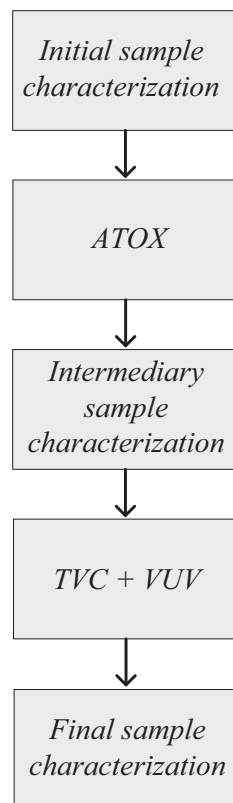Fig. 10. Thermal cycle with temperatures from +150 °C to −150 °C.

Fig. 11. LEO samples test flow.

and mass determination; the text box "*TVC + VUV*" addresses the samples exposure to thermal vacuum cycling and vacuum ultra-violet respectively; the text box *Final sample characterization* is the final inspection of the

material sample for evaluation by photos and mass determination.

5.2. Materials selection

The selected materials were the most commonly used in LEO satellites, i.e. the most representative outer materials of the satellite are paints and MLI blankets. Nine samples of paints and of MLI were selected and subject to space evaluation testing.

- *Paints*

One of the paints main tasks is to support the spacecraft thermal control. This is achieved by the reflection or absorption of electromagnetic radiation from the sun, while also taking the ability to heat conduction. Spacecraft passive thermal design allows thermal energy channels along the exterior, so that appropriate temperatures are maintained in the various elements of the spacecraft. Also, another important aspect of the paint is the electric conductivity, by avoiding electric charges/discharge formation, i.e., with ESD protection.

The paints selection criteria were the following: 1) Used outside satellite; 2) Most used paints; 3) Study of different base composition paints; white or black paints. The preferred paints are given in Table 2.

The paintings have been applied by MAP on Au4G (aluminum alloys substrate) and CFRP. The CFRP substrates (reference M55J/RS3M) have been provided by ONERA, France. The procedure for application done by MAP was: Milling of surface (rough side for CFRP); Cleaning; Spraying of paintings; Curing.

Table 2
Preferred paints.

Sample	Material/Substrate	Notes
LEO paint 1	PSB/CFRP	Silicate white paint applied on CFRP
LEO paint 2	PUK/CFRP	Polyurethane black applied on CFRP
LEO paint 3	SG121FD/CFRP	Silicone white paint applied on CFRP
LEO paint 4	PUK/Alu	Polyurethane black applied on Au4G substrate with 3 slashes
LEO paint 5	SG121FD/Alu	Silicone white paint applied on Au4G substrate with 3 slashes
LEO paint 6	PSB/Alu	Silicate white paint applied on Au4G substrate with 3 slashes

- *MLI*

The MLI is the ultimate in high performance insulation. The MLI specifically addresses all modes of heat transfer through the basic design of the system. The reflective shields are used to minimize radiation, once heat transfer is inversely proportional to the number of shields. The low conductivity spacers are used to prevent the metallic based reflective shields from touching and also minimizes the heat transfer through the blanket itself. Much care is required when designing the MLI blanket, once it should minimizes the heat transfer in all ways, including through edges and seams. The MLI blankets were provided by RUAG, Switzerland. The RUAG LEO MLI blankets Lay-Ups is shown in Fig. 12.

The LEO MLI 1 blankets and LEO MLI 3 blankets samples were attached with velcros (reference SJ3571 Nylon 6.6). The velcros were assembled on Au4G substrate sample with size 48.9 mm × 48.9 mm. The MLI sample size 46 mm × 46 mm. The LEO MLI 2 was sample was attached with double side PSA on Au4G substrate size 48.9 mm × 48.9 mm.

5.3. Test specifications

- *ATOX specifications*

During the ATOX test, the flux and fluence was calculated/measured, i.e., by measuring the mass loss of the witness sample position at the center of the sample holder. The ATOX fluence was 9.2e+20 Atoms/cm^2 with an exposure time value of 434100 s and the flux value during the test was 2.11e+15 Atoms/cm^2 s. The flux and fluence was estimated from the mass loss of Kapton.

The ATOX total fluence per sample considering uniformity and test fluence and equivalent space time is shown in Table 3.

In Table 3 is considered: NRLMSISE-00 spenvis model, values of high solar activity; F10.7 (daily) 250; F10.7 (average) 250; AP 45; +75°; Front fluence.
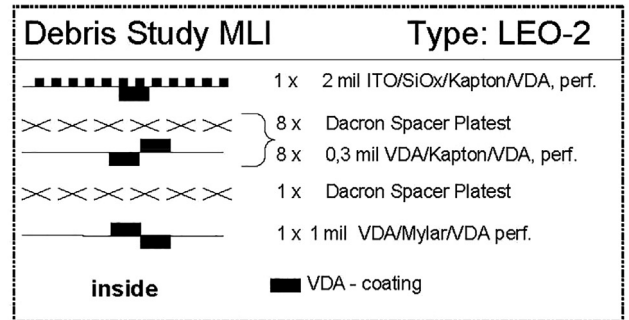
- *TVC specifications*

The TVC conditions were: 1) High temperature +140 C; 2) Low temperature −120 C; 3) Dwell time 10 min; 4) Time per cycle 4.13 h; 5) 500 cycles.
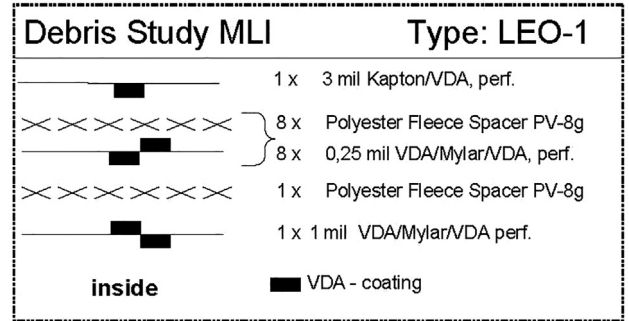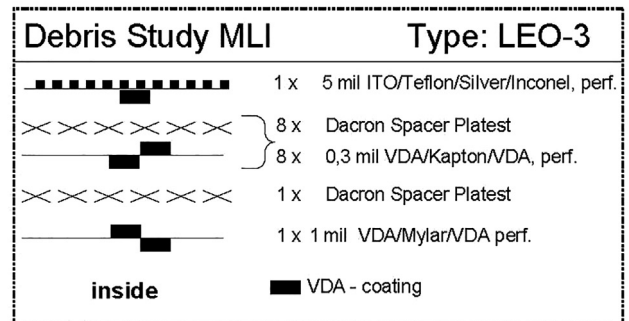

Fig. 12. RUAG LEO MLI blankets Lay-Ups.

The TVC temperatures: blue line is the sample holder temperature shown in Fig. 13.

- *VUV specifications*

The VUV specifications were: average number of suns during the test: 2.4 ± 0.2; ESH at center of exposure 5145 ESH.

Table 3
Total fluence per sample and ATOX mission year equivalent per sample type. EMY (equivalence on mission years).

Sample reference	Description	Fluence	Equivalent mission years			
			745 km, ±75°	(800 Km, ±75°	900 km, ±75°	1000 km, ±75°
LEO MLI1	3 mil Kapton/VDA	7.62e+20	4.6	8.1	21.1	54.4
LEO MLI2	2 mil ITO/SiOx/Kapton/VDA	1.00e+21	6.2	10.6	27.7	71.4
LEO MLI3	5 mil ITO/Teflon/Silver/Inconel	7.78e+20	4.7	8.3	21.5	55.5
LEO Paint 1	PSB/CFRP	8.00e+20	4.8	8.5	22.2	57.1
LEO Paint 2	PUK/CFRP	9.13e+20	5.5	9.7	25.3	65.2
LEO Paint 3	SG121FD/CFRP	8.96e+20	5.4	9.5	24.8	64.0
LEO Paint 4	PUK/Alu	1.01e+21	6.1	10.7	28.0	72.1
LEO Paint 5	SG121FD/Alu	9.89e+20	5.9	10.5	27.4	70.6
LEO Paint 6	PSB/Alu	6.33e+20	3.8	6.7	17.5	45.2
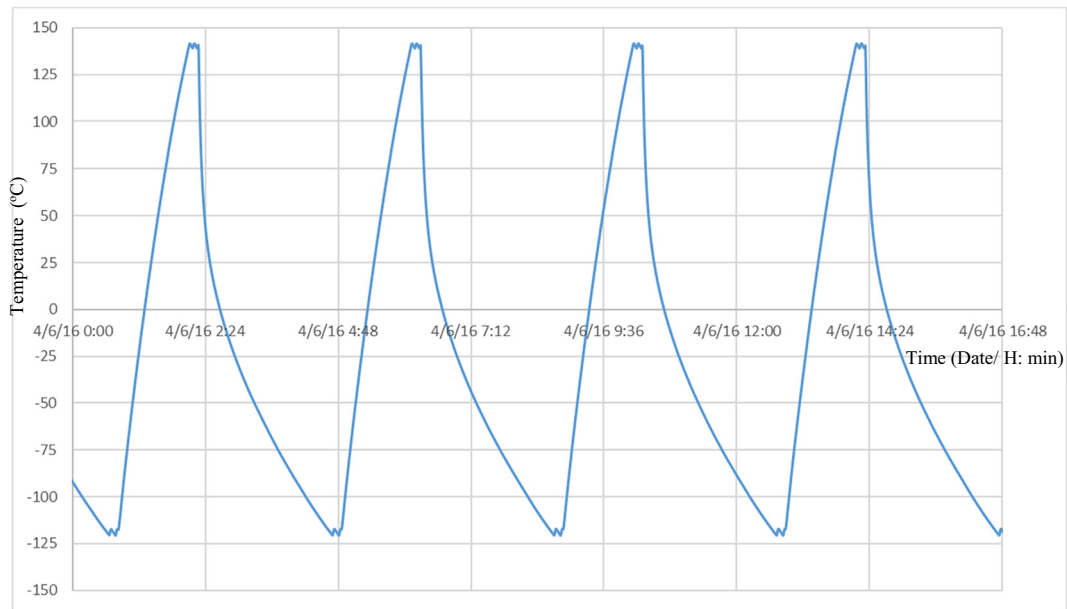
Fig. 13. TVC temperatures: blue line is the sample holder temperature. (For interpretation of the references to colour in this figure legend, the reader is referred to the web version of this article.)
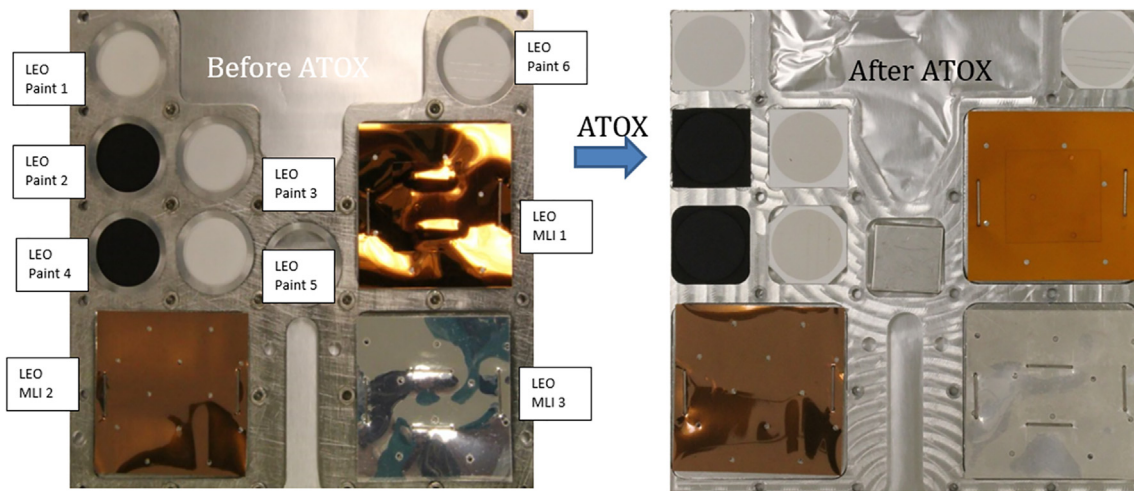

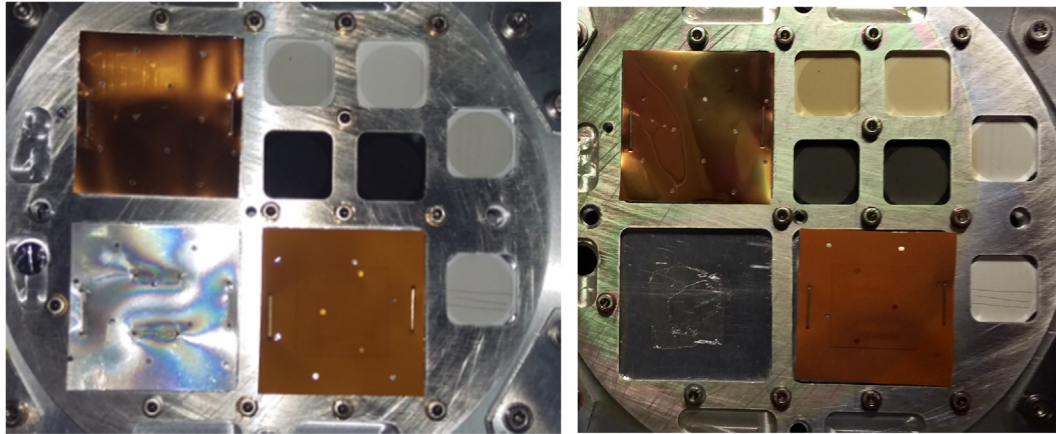Fig. 14. Samples before (left) and after (right) ATOX test.

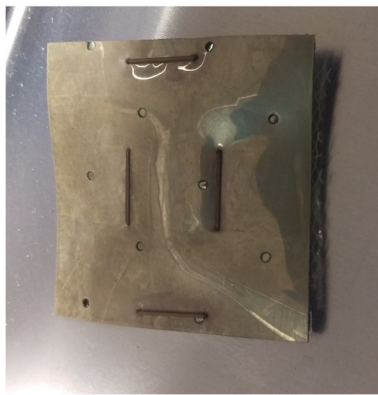Fig. 15. Samples of Velcro before (left) and after (right) TVC + VUV test.

Fig. 16. LEO MLI 3 on the tray below the sample holder.

5.4. Results

During the tests flaking of paints and generation of micron sized debris particles from the MLI were observed. Additionally, the velcro used as MLI fixation and the MLI materials were strongly degraded. The samples materials used, before and after ATOX exposure are shown in Fig. 14.

In Fig. 14 can be seen that in all that the isolator material behind the venting halls is severely destroyed by the ATOX test. As expected MLI 2 that have in the external layer is highly resistant to ATOX. This is the less effected by the all test campaign. ATOX affect considerably the Kapton of the MLI 1, i.e., Kapton external layer and the MLI 3, i.e., ITO external layer.

After ATOX test the samples were exposed to VUV + TVC test. The samples materials, i.e., velcro used, before (left) and after (right) TVC + VUV test are shown in Fig. 15.

The MLI 3 fall down during cooldown (cycle 433) due to PSA failure is shown in Fig. 16.

The mass loss measurements are presented in Table 4.

In the Table 4, there are two cases that the mass increased after TVC + VUV test, i.e., LEO Paint 1 and LEO MLI 3, due to a possible absorption of atmosphere gases (e.g. moister) by the samples after being removed from vacuum.

The MLI first layer density values: MLI 1 density is $1.08e-4$ g/mm^2; MLI 2 density is $7.39e-5$ g/mm^2; MLI 3 density is $2.87e-4$ g/mm^2. Paint densities values are: PUK: 1.23 g dry/m^2/μm; PSB: 4 g dry/m^2/μm; SG121FD: 1.87 g dry/m^2/μm.

Table 4
Sample weight variation.

Sample number	Description	Dimensions of substrates (mm)	Initial mass (g)	Mass after ATOX (g)	ATOX mass loss (g)	Mass after ATOX + TVC VUV (g)	Total mass loss (g)
LEO Paint 1	PSB/CFRP	$22 \times 22 \times 0.6$	0.443	0.4427	$-3.00e-04$	–	–
LEO Paint 2	PUK/CFRP	$22 \times 22 \times 0.6$	0.4038	0.4013	$-2.50e-03$	0.3968	$7e-3$
LEO Paint 3	SG121FD/CFRP	$22 \times 22 \times 0.6$	0.4998	0.4996	$-2.00e-04$	0.4387	$6.1e-2$
LEO Paint 4	PUK/Alu	$21.9 \times 21.9 \times 4.1$	4.8313	4.8288	$-2.50e-03$	4.7180	$1.13e-1$
LEO Paint 5	SG121FD/Alu	$21.9 \times 21.9 \times 4.1$	4.8197	4.8194	$-3.00e-04$	4.8157	$4e-3$
LEO Paint 6	PSB/Alu	$21.9 \times 21.9 \times 4.1$	4.7562	4.756	$-2.00e-04$	4.7544	$1.8e-3$
LEO MLI 1	3 mil Kapton/VDA	46.5×46.5	21.5637	21.4869	$-7.68e-02$	21.4828	$8.1e-2$
LEO MLI 2	2 mil ITO/SiOx/Kapton/VDA	46.5×46.5	19.428	19.4269	$-1.10e-03$	19.4136	$1.4e-2$
LEO MLI 3	5 mil ITO/Teflon/Silver/Inconel	46.5×46.5	21.4432	21.4385	$-4.70e-03$	–	–
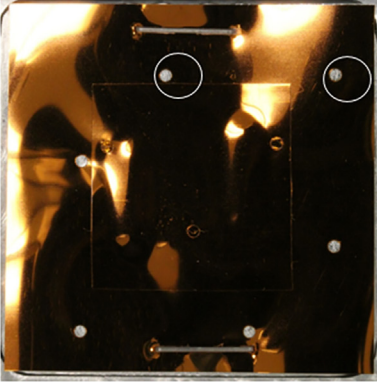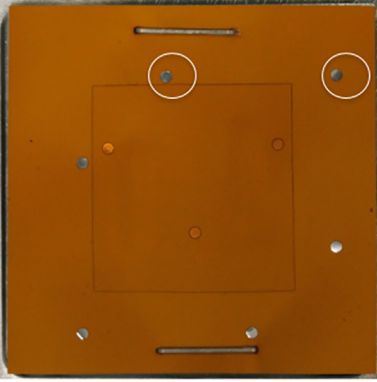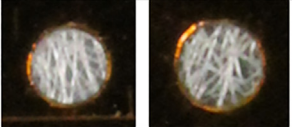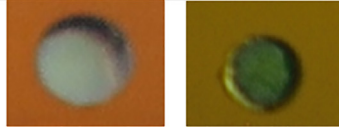
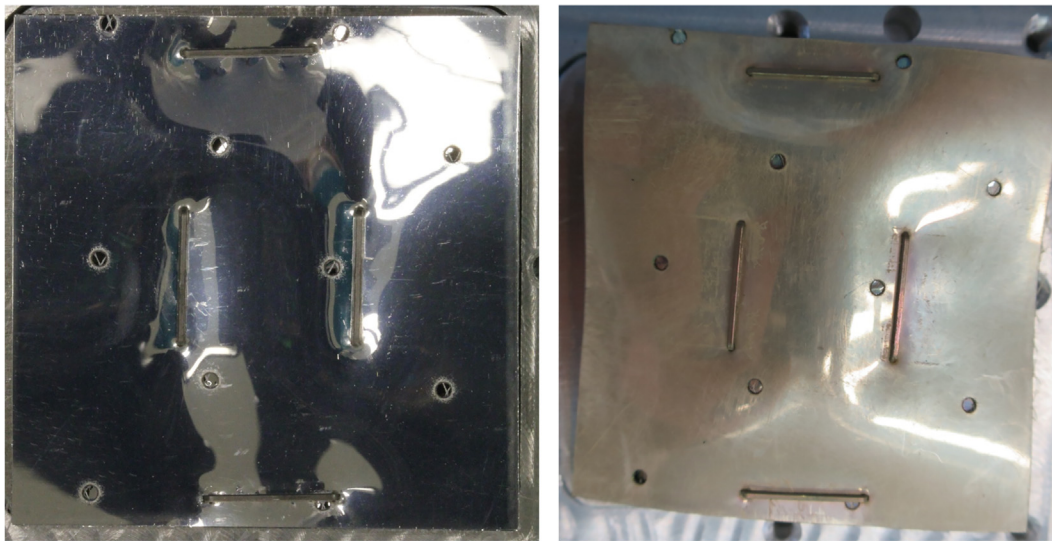Fig. 17. MLI 1 degradation before (left) and after (right) tests.

Fig. 18. LEO MLI 3, before (left) and after (right) the test.

Fig. 19. MLI side view. It can be seen the strong degradation of the velcro.

The MLI 1 degradation during the test is shown in Fig. 17.

The LEO MLI 3 before (left) and after testing (right) are shown in Fig. 18.

The MLI side view. It can be seen the strong degradation of the velcro shown in Fig. 19.

All MLI became curved after TC. Main reason of this effect is the deformation (shrinkage) of the Velcro (see image below) and of the PSA.

Regarding paints, flanking was observed on LEO paint 1 PSB/CFRP and on, LEO paint 4 PUK/Alu. The LEO paint 4 flaking is shown in Fig. 20.

Considering Fig. 20 the area of the paint flakes of paint 1 and of paint 4 are presented in Table 5 and Table 6 respectively.
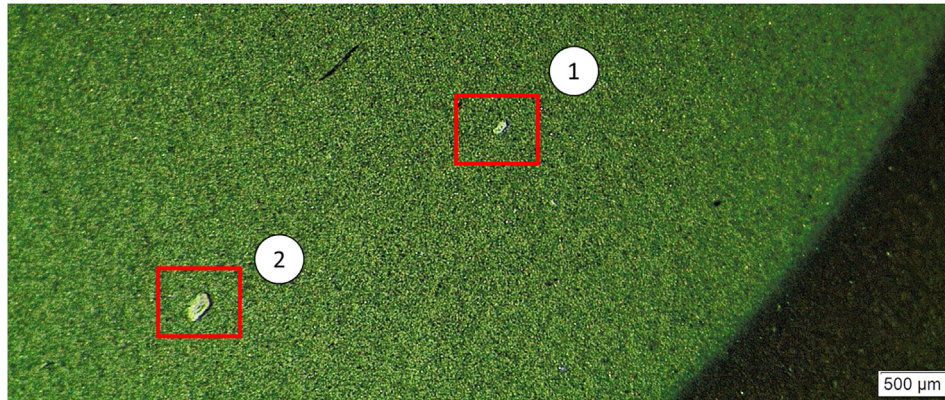
Fig. 20. LEO paint 4 flaking.

Table 5
Flaking area from LEO Paint 1 PSB/CFRP.

	Flaking area (μm^2)
1	6300
2	7400
3	2000
4	4100
5	5600
6	3500
7	3300

Table 6
Flaking area from LEO paint 4 PUK/Alu.

	Flaking area (μm^2)
1	15,000
2	36,000
3	18,000

6. Conclusion

In this paper is reported the conception and experimental setup of a new concept for a Vacuum Ultraviolet with extreme Thermal Vacuum Cycle system, based on a Helium cryocooler technology, a mechanical thermal switch, and a VUV lamp. The system was dimensioned, assembled and its performance characterized.

The system is able to generate TVC with a range of ±150 °C. Each TVC cycle takes about 5 h, for this temperature range. The VUV system can illuminate a 150 mm diameter area with 3.89 suns.

A major constrain is the cooper brads, that limited the heat transfer, increasing the duration of a cycle. A bigger section of the brads or a short length could not be implemented due to systems constrains.

The system is now operational has been used for ESA studies and is ready for any further studies.

The synergistic effects of radiation, VUV, thermal cycling and ATOX in several spacecraft materials was investigated. Materials degradation process that lead to debris formation (e.g. paint flaking, MLI mylar layers and velcro became very fragile) were observed.

After testing, it was observed that some paints change their thermo-optical properties and started to flake. The PSA used to glue the velcros to the spacecraft and also to glue directly some MLIs to the spacecraft's tends to fail, i.e., velcros lose their adhesive properties on over the overstress temperature range. The failure of PSA was also observed during the cooldown cycle.

This suggest that in a scenario were a satellite has lost its thermal shielding capability, the failure of PSA and loss of Velcro properties, it may contribute to the release of the full MLI blanket (depending of the fixation methods).

Also, After expose the MLIs to LEO test conditions it was observed that MLI become stiffer. This suggests that MLI materials can become more susceptible when subjected to High Velocity Impacts.

Acknowledgement

References

Anwar, A., Osman, M., Elfiky, D., Hassan, G.M., 2018. Performance evaluation of selected irradiated space structure composites manufactured by the hand lay-up method. Int. Rev. Aerospace Eng. 11 (4), 155–161.

Banks, B.A., de Groh, K.K., Miller, S.K., 2004. Low Earth Orbital Atomic Oxygen Interactions with Spacecraft materials. National Aeronautics Space Administration, USA.

Clair, A.K. St, Slemp, W.S., Clair, T.L. St, 1980. High-temperature adhesives for bonding polyimide film, Report TM-81824. National Aeronautics Space Administration, USA.

ESA Project, 2017, Space debris from spacecraft degradation products; European Space Agency, Project Contract 4000113047/14/NL/LF/TU-IAS, link: https://indico.esa.int/event/188/contributions/1663/.

Flegel, S.K., Gelhaus, J., Möckel, M., Wiedemann, C., Krag, H., Klinkrad, H., Vörsmann, P., 2011. Multi-layer insulation model for master-2009. Acta Astronaut. 69, 911–922.

Fayazbakhsh, K., Abedian, A., 2010. Materials selection for applications in space environment considering outgassing phenomenon. Adv. Space Res. 45, 741–749.

Frederico, T., 2017, Development of a cryogenic facility for the generation of space debris. MSc Thesis, Faculdade de Ciências, Universidade de Lisboa, Portugal.

Gordo, P, 2017, Space debris from spacecraft degradation products, ESA-CNES Radiation Final Presentation: 6 Mar 2017; https://indico.esa.int/event/188/contributions/1663/.

Gouzman, I., Girshevitz, O., Grossman, E., Eliaz, N., Sukenik, C.N., 2010. Thin film oxide barrier layers: protection of kapton from space environment by liquid phase deposition of titanium oxide. ACS Appl. Mater. Interfaces 2 (7), 1835–1843.

Kiefer, R.L., Orwoll, R.A., 1987, Space environment effects on polymeric materials", Nasa technical report NAG-1-678.

Mori, K., Ishizawa, J., 2013. Temperature effects of ultraviolet irradiation on material degradation. Protection of Materials and Structures from the Space Environment, vol. 32. Springer, Berlin, Heidelberg, pp. 399–407.

Navick, X.-F., Carty, M., Chapellier, M., Chardin, G., Goldbach, C., Granelli, R., Hervé, S., Karolak, M., Nollez, G., Nizery, F., Riccio, C., Starzynski, P., Villar, V., 2004. Fabrication of ultra-low radioactivity detector holders for Edelweiss-II. Nucl. Instrum. Methods Phys. Res., Sect. A 520 (1–3), 189–192.

Pascoal, D.G., 2016, Development and validation of the ultraviolet light system (UV and VUV) of satellite coverage deterioration simulation infrastructure. MSc Thesis, in Portuguese, Faculdade de Ciências, Universidade de Lisboa, Portugal.

Samwel, S.W., El-Aziz, E.A., Garrett, H.B., Hady, A.A., Ibrahim, M., Amin, M.Y., 2019. Space radiation impact on smallsats during maximum and minimum solar activity. Adv. Space Res. 64, 239–251.

Silverman, E.M., 1995. Space environmental effects on spacecraft: LEO materials selection guide, part 1, Report 4661. National Aeronautics Space Administration, USA.

Tighe, A.P., Iwanosky, B., van Eesbeek, M., Duzellier, S., Dinguirard, M., Falguere, D., Pons, C., Inguimbert, V., Rejsek, V., Durin, C., Mandeville, J.C., Gabriel, S., Goulty, D., Roberts, G., 2009. Overview of results from the materials exposure and degradation experiment (MEDET) after 18 months in orbit on the ISS. Proc. 11th International Symposium on Materials in a Space Environment-ISMSE, 15-18 September 2009, Aix en Provence, France, pp. 1–10.

Williamson, M., 2004. Protection of the space environment: the first small steps. Adv. Space Res. 34, 2338–2343.